Asymmetric chromatin capture and nuclear envelopes separate endogenous and ectopic chromosomes after induced cell fusion

Bharath Sunchu [1], Nicole Lee [1,2], Roberto Carlos Segura[1] & Clemens Cabernard [1]

[1] Department of Biology, University of Washington
Life Science Building
Seattle, Washington State, USA

Current address:

[2] Cancer Science Institute, National University of Singapore
Singapore

[*] Lead and corresponding author: ccabern@uw.edu

Metazoan cells accurately attach to, congress and segregate chromosomes during mitosis Additionally, hybrid cells derived through fertilization or somatic cell fusion also employ mechanisms to recognize and separate chromosomes of different origin. The underlying mechanisms are mostly unknown but could prevent aneuploidy and tumor formation. Here, we acutely induce fusion between *Drosophila* neural stem cells (neuroblasts) and differentiating ganglion mother cells (GMCs) *in vivo* to define how epigenetically distinct chromatin is recognized and segregated. We find that Nb-GMC hybrid cells align both endogenous (neuroblast-origin) and ectopic (GMC-origin) chromosomes at the metaphase plate through centrosome derived dual spindles. Mixing of endogenous and ectopic chromatin is prevented through an asymmetric, microtubule-dependent chromatin capture mechanism during interphase and physical boundaries imposed by nuclear envelopes. Although hybrid cells fail to accurately segregate ectopic chromatin, manifested in lagging chromosomes and chromosome bridges, transplanted brain tissue containing hybrid cells neither reduce the lifespan nor form visible tumors in host flies. We conclude that fly neural stem cells utilize asymmetric centrosome activity in interphase to capture and physically separate epigenetically distinct chromatin in a microtubule-dependent manner. We propose a novel chromosome recognition and separation mechanism that could also inform biased chromatid segregation observed in flies and vertebrates.

Dividing cells distribute replicated chromosomes equally between the two forming sibling cells through microtubule-dependent attachment and segregation mechanisms (McIntosh, 2016; Maiato et al., 2017). Chromosomes are connected with microtubules via kinetochore proteins, which are localized on centromeric DNA (Thomas et al., 2017; Yu et al., 2019). The occurrence of biased segregation of sister chromatids or homologous chromosomes during mitosis and meiosis

69 respectively, as well as the spatial separation of the maternal and paternal genomes during early
70 vertebrate development, implies the presence of accurate chromatin recognition mechanisms
71 (Akera et al., 2017; Ranjan et al., 2019; Sunchu and Cabernard, 2020; Reichmann et al., 2018).
72 Chromosome separation has also been observed in fused human cells (Heasley et al., 2017; Rieder
73 et al., 1997). The molecular nature of these separation mechanisms is unclear but could entail
74 asymmetries in centromere binding proteins, kinetochore size or kinetochore composition (Arco et
75 al., 2018; Ranjan et al., 2019; Akera et al., 2019; Drpic et al., 2018).
76 Over a century ago, cell – cell fusion has also been proposed to initiate tumor formation (Aichel,
77 1911), possibly through chromosome missegregation and aneuploidy (Boveri, 2008; Molina et al.,
78 2020). Here, we ask how hybrid cells accurately recognize, separate and segregate epigenetically
79 distinct chromosomes. To this end, we acutely fused *Drosophila* neural stem cells (neuroblasts
80 (NBs), hereafter) with differentiating ganglion mother cells (GMCs) in the intact larval fly brain
81 to create hybrid cells, containing both neuroblast and GMC chromosomes. Unperturbed *Drosophila*
82 neuroblasts divide asymmetrically, self-renewing the neural stem cell while forming a
83 differentiating GMC. Neuroblasts are twice the size of GMCs and neurons and express the
84 transcription factor Deadpan (Dpn^+), whereas GMCs and neurons can be identified based on
85 Prospero ($Pros^+$) expression (Gallaud et al., 2017) (Fig. S1A). We used a 532nm pulsed laser to
86 induce a small lesion at the Nb – GMC interface between a dividing neuroblast and GMC, causing
87 the GMC chromatin to enter the neuroblast cytoplasm. Targeted mitotic neuroblasts often retain
88 the GMC chromosomes, creating a large apical hybrid cell containing a Dpn^+ and $Pros^+$ nucleus
89 (Nb – GMC hybrid). Most Nb – GMC hybrid cells normally localize the contractile ring marker non-
90 muscle Myosin to the cleavage furrow and complete cytokinesis (Fig. S1B-E). Acute cell fusion can
91 also result in the expulsion of the GMC chromatin, forming GMC – GMC hybrids (see

92 Supplementary Fig. 3c in (Roubinet et al., 2017)) but the focus here is on Nb – GMC hybrids
93 (hybrid cells, hereafter) only.
94
95 To better characterize the dynamics of neuroblast (endogenous) and GMC (ectopic)
96 chromosomes during mitosis, we induced cell fusion at different cell cycle stages in wild type
97 neuroblasts, expressing the canonical chromosome marker His2A::GFP. Hybrid cells derived from
98 Nb-GMC fusions early in the cell cycle could (1) align only the neuroblast chromosomes at the
99 metaphase plate, (2) congress a mix of neuroblast and GMC chromosomes or (3) separate and
100 align the two chromosome pools at the metaphase plate (Fig. 1A). We found that the endogenous
101 and ectopic chromatin was separated and distinguishable when fusions were induced in early
102 mitosis. Both the ectopic and endogenous chromatin aligned at the metaphase plate (Fig. 1B; video
103 1&2). Nb-GMC fusions can be induced at all cell cycle stages but GMC chromosomes align at the
104 metaphase plate more accurately in hybrid cells derived from interphase or early prophase fusions
105 (Fig. 1C, D). We conclude that hybrid cells derived from fusions between interphase Nbs and non-
106 mitotic GMCs accurately align ectopic and endogenous chromatin at the metaphase plate.
107
108 **Nb-GMC hybrid cells independently align Nb and GMC chromatin at the metaphase plate**
109 We next asked whether GMC chromatin congresses independently of neuroblast chromatin. To this
110 end, we measured the time between nuclear envelope breakdown (NEB) and chromosome
111 alignment at the metaphase plate for Nb and ectopic GMC chromatin in hybrid cells derived from
112 interphase and early prophase fusions (Fig. 1E). In most hybrid cells, ectopic and endogenous
113 chromatin was distinguishable based on differences in location and intensity (see Fig. 1B; video
114 1&2). In untargeted control neuroblasts (unfused), Nb chromosomes aligned at the metaphase
115 plate within 6.5 minutes after NEB (SD = 1.55; n = 6), which is insignificantly faster than the

116 neuroblast chromosomes of hybrid cells (t = 6.9 mins; SD = 2.84; n = 11). GMC chromosomes
117 aligned within 7.63 mins (SD = 3.69; n = 11), statistically not significantly different from
118 unperturbed wild type chromosomes (Fig. 1E). In most Nb-GMC hybrids, the endogenous
119 neuroblast and the ectopic GMC chromosomes aligned at the metaphase plate with no significant
120 time difference. However, in a few cases, ectopic chromatin aligned before or after the neuroblast
121 chromatin (Fig. 1F). These results suggest that the neuroblast and GMC chromatin can move
122 independently to the metaphase plate in hybrid cells.
123

124 **Ectopic spindles distinguish between Nb and GMC chromatin**

125 We next investigated the mechanisms underlying independent Nb/GMC chromosome alignment.
126 Ectopic chromosomes could be aligned together with the endogenous chromosomes via a single
127 bipolar spindle. Alternatively, hybrid cells could form multiple bipolar spindles, which attach to
128 either the neuroblast's, GMC's, or chromosomes from both cell types (Fig. 2Aa). Live cell imaging
129 showed that hybrid cells derived from interphase Nb-GMC fusions contained double spindles in
130 almost all cases, whereas the vast majority of cell fusions induced in metaphase only formed one
131 mitotic spindle (Fig. 2B, C & video 3). Most hybrid cells contained two mitotic spindles, which
132 predominantly formed at the same time (Fig. 2D, E). We quantified spindle alignment and
133 positioning dynamics by measuring the angle and distance between the two spindles during
134 metaphase (Fig. 2F and methods). The two spindles were initially misaligned and separated but
135 decreased their inter-spindle distance and angle during metaphase (Fig. 2G-I). We conclude that
136 Nb-GMC hybrid cells align neuroblast and GMC chromosomes separately at the metaphase plate
137 through the formation of independent mitotic spindles.
138

139 **Ectopic spindles are nucleated from GMC centrosomes**

140 Mitotic spindles can be nucleated through the centrosome-dependent, chromatin or microtubule
141 pathway but when centrosomes are present, the centrosome pathway prevails (Prosser and
142 Pelletier, 2017). To elucidate the mechanisms underlying ectopic spindle formation, we induced
143 Nb-GMC fusions in interphase wild type neuroblasts expressing a live centriole (Asterless;
144 Asl::GFP) and spindle marker (cherry::Jupiter), and assayed centrosome dynamics and spindle
145 formation throughout mitosis. Normal wild type neuroblasts usually contain two Asl::GFP positive
146 centrioles in mitosis, forming a single bipolar spindle. However, in Nb-GMC hybrids, we
147 predominantly found four Asl::GFP positive centrioles, two of which seemed to be introduced from
148 the GMC (Fig. 2J,K). The GMC centrosomes nucleated an ectopic bipolar spindle that subsequently
149 aligned with the main neuroblast spindle. Although multipolar spindle formation can be prevented
150 through centrosome clustering (Quintyne et al., 2005), we observed that GMC centrosomes
151 approached neuroblast centrosomes but still formed two parallel bipolar spindles. We conclude
152 that ectopic spindles are formed through the centrosome pathway, using centrioles originating
153 from GMCs.
154
155 **Microtubule-dependent, asymmetric chromatin-centrosome attachments retain**
156 **chromosomes close to the apical neuroblast cortex during interphase**
157 Our data suggest that Nb and GMC chromatin are being separated through an endogenous, Nb-
158 derived and an ectopic, GMC-derived mitotic spindle. We next investigated how these spindles
159 distinguish between Nb and GMC chromosomes. During mitosis, microtubules emanate from
160 centrosomes and attach to sister chromatids through kinetochore proteins, localizing to the
161 centromeric region (Fukagawa and Earnshaw, 2014). *Drosophila* male germline stem cells contain
162 asymmetric levels of the centromere-specific H3 variant (Centromere identifier (Cid) in flies
163 (Henikoff et al., 2000)) (Ranjan et al., 2019), prompting us to investigate whether Cid intensity

differs between endogenous and ectopic chromatin in hybrid cells. We induced Nb-GMC fusions of wild type cells expressing Cid::EGFP (Ranjan et al., 2019) and measured Cid intensity on both GMC and Nb chromatin. These measurements did not reveal a significant intensity difference between Nb and GMC Cid (Fig. S2A). However, we noticed that endogenous Cid::EGFP was localized in very close proximity to the apical centrosome in unperturbed interphase and prophase wild type neuroblasts (Fig. S2B & video 4). Cid::EGFP remained associated with chromatin throughout the neuroblast cell cycle, excluding the possibility that early Cid clusters are not connected with chromatin (Fig. S2F & video 5).

Interphase wild type neuroblasts contain only one active apical microtubule organizing center (MTOC), retaining the daughter-centriole containing centrosome close to the apical neuroblast cortex. The mother-centriole-containing centrosome is inactive in interphase but matures from prophase onward, positioning itself on the basal cell cortex (Januschke et al., 2013, 2011; Januschke and Gonzalez, 2010; Gallaud et al., 2020). We measured the distance of individual Cid::EGFP clusters to the apical and basal centrosome in unperturbed wild type neuroblasts (Fig. S 2C) and found that interphase Cid was always in close proximity to the apical centrosome. After nuclear envelope breakdown (NEB), Cid moved progressively towards the metaphase plate (Fig. S 2D). Once the basal centrosome appeared (0 mins), Cid was still closer to the apical than the basal centrosome and this distance asymmetry was still intact 6 minutes after the appearance of the basal centrosome (Fig. S2E).

The proximity of Cid::EGFP clusters to the active interphase MTOC suggests a microtubule-dependent chromosome attachment mechanism. Indeed, wild type neuroblasts treated with the microtubule-depolymerizing drug colcemid showed a strong correlation between apical MTOC activity and Cid localization; as MTs depolymerize after colcemid addition, Cid progressively moved away from the apical cortex towards the cell center (Fig. S2G, H & video 6). To test whether

188 MTOCs are connected to Cid clusters during interphase, we removed the centriolar protein
189 Centrobin (Cnb; CNTROB in humans). Neuroblasts lacking Cnb fail to maintain an active apical
190 interphase MTOC but regain normal MTOC activity during mitosis (Januschke et al., 2013).
191 Neuroblasts expressing *cnb* RNAi lost apical Cid localization after the apical centrosome
192 downregulated its MTOC activity. However, maturing centrosomes reconnected with Cid in
193 prophase (Fig. S2I, J & video 7). Cid's proximity to the apical MTOC ('apical' refers to the
194 centrosome destined to move to the apical cortex) in *cnb* RNAi expressing neuroblasts was much
195 more varied compared to wild type (Fig. S2L). At 6 minutes after centrosome maturation onset,
196 Cid – apical MTOC distance was comparable to wild type, as were Cid – basal centrosome distance
197 relationships (Fig. S2K-M). We conclude that Cid-containing chromatin is already attached to the
198 apical centrosome prior to entry into mitosis.
199

200 **Asymmetric centrosome-chromatin attachments contribute to the separation of**
201 **endogenous and ectopic chromosomes**

202 Based on these observations, we hypothesized that the separation between endogenous and
203 ectopic chromosomes could be due to a pre-attachment mechanism, preventing mixing of Nb and
204 GMC chromosomes. To test this hypothesis, we first analyzed Cid localization in relation to the
205 endogenous and ectopic centrosomes in wild type hybrid cells. Similar to unperturbed wild type
206 neuroblasts, endogenous Cid is also localized in close proximity to the endogenous apical
207 centrosome in wild type hybrid cells (Fig. 3A-C, G, H & video 8; 'apical' refers to the centrosome
208 destined to segregate into the large apical sibling cell) and appeared further away from ectopic
209 Cid clusters compared to ectopic centrosomes (Fig. 3A-C, I & video 8; 0 mins refers to the
210 appearance of the endogenous basal centrosome; '0' refers to the appearance of the ectopic
211 centrosomes).

212 We next attempted to randomize Cid – centrosome distance relationships by inducing acute fusions
213 in *cnb* RNAi expressing neuroblasts, since loss of interphase MTOC activity released endogenous
214 Cid from the apical centrosome (see above; Fig. S2G-M). In contrast to wild type hybrid cells,
215 endogenous Cid is roughly equidistant to the endogenous and ectopic centrosomes in *cnb* RNAi
216 expressing hybrid cells at 0 mins and '0' mins respectively (Fig. 3D-F, J, K & video 9). However,
217 ectopic Cid was still closer to the ectopic centrosomes in *cnb* RNAi expressing hybrid cells compared
218 to the endogenous apical centrosome (Fig. 3D, F, L & video 9). In both wild type and *cnb* RNAi
219 expressing hybrid cells, ectopic and basal centrosomes were about equidistant to endogenous Cid,
220 but ectopic centrosomes were closer to ectopic Cid (Fig. S3A-D). Taken together, we conclude that
221 in hybrid cells the apical MTOC forms an asymmetric attachment to endogenous Cid-containing
222 chromosomes prior to entry into mitosis.
223
224 **Nuclear envelopes separate ectopic and endogenous chromatin in hybrid cells**
225 We next asked whether early MTOC – Cid attachments are sufficient to prevent endogenous and
226 ectopic chromosome separation, tracking endogenous and ectopic Cid::EGFP after induced cell
227 fusion. In wild type hybrid cells, endogenous and ectopic CID clusters started to congress at the
228 metaphase plate and became difficult to clearly separate 8.8 mins (SD = 5.63; n = 5; Fig. 3M)
229 after NEB. However, 50% of *cnb* RNAi hybrid cells showed endogenous and ectopic Cid mixing
230 prior to NEB (Fig. 3D, N), although the time difference was not significantly different to wild type
231 hybrid cells (Fig. 3M).
232 Neuroblasts undergo semi-closed mitosis, mostly retaining a matrix composed of nuclear
233 envelope proteins around the mitotic spindle (Katsani et al., 2008). We imaged hybrid cells with
234 the nuclear envelope marker Klaroid, using the protein-trap line koi::EGFP (Buszczak et al., 2007).
235 We confirmed that unperturbed wild type neuroblasts contain a nuclear envelope matrix

236 surrounding the mitotic spindle during mitosis (Fig. S3E). Similarly, wild type hybrid cells contain
237 two nuclear envelopes during mitosis (Fig. 3O and Fig. S3F). Taken together, these data suggest
238 that asymmetric MTOC-Cid attachments in interphase and nuclear envelopes establish and
239 maintain the physical separation between endogenous and ectopic chromosomes in hybrid cells.
240 Loss of biased interphase MTOC activity removes asymmetric MTOC-Cid attachments and allows
241 for cross-connections between endogenous centrosomes and ectopic Cid (Fig. 3P).
242

243 **Hybrid cells segregate endogenous and ectopic chromosomes independently**

244 We next investigated whether both bipolar spindles are functional in Nb-GMC hybrid cells.
245 Erroneous or incomplete microtubule-kinetochore attachments trigger the spindle assembly
246 checkpoint (SAC), preventing or delaying anaphase entry (Musacchio, 2015). Since the
247 kinetochore-derived 'wait anaphase' signal is diffusible (Heasley et al., 2017), ectopic spindles
248 should thus also obey the SAC in Nb-GMC hybrid cells. We tested whether hybrid cells contain
249 functional microtubule-kinetochore attachments by measuring the time between finished
250 chromosome alignment at the metaphase plate and chromosome separation in Nb-GMC hybrids
251 expressing His2A::GFP and cherry::Jupiter (Fig. 4A, B). Unperturbed control neuroblasts usually
252 initiate anaphase onset within 2.63 minutes (SD=1.84; n=12) after chromosomes are aligned at
253 the metaphase plate. In hybrid cells derived from interphase fusions, endogenous and ectopic
254 chromatin entered anaphase 4.14 mins (SD= 2.23; n=14) and 5.12 minutes (SD= 1.85; n=13)
255 after metaphase alignment. Only ectopic chromatin for prophase induced hybrid cells showed a
256 significantly delayed anaphase onset (Average: 10.25 mins; SD= 4.12; n=6) (Fig. 4C). Ectopic
257 chromatin never separated before endogenous chromosomes but entered anaphase with a few
258 minutes delay (Fig. 4D). We conclude that in Nb-GMC hybrids, endogenous and ectopic
259 chromosomes establish correct MT-kinetochore attachments, thereby fulfilling the spindle

260 assembly checkpoint necessary to enter anaphase. However, given the delays in ectopic
261 chromosome separation, we further conclude that ectopic spindles can initiate chromatid
262 separation independently from the endogenous neuroblast spindle.
263
264 **Hybrid cells are insufficient to induce tumors in wild type host flies**
265 Finally, we assessed the accuracy of chromosome segregation in wild type hybrid cells. Using the
266 canonical chromosome marker His2A::GFP we detected chromosome missegregation - ranging
267 from lagging chromosomes to chromosome bridges - in all wild type hybrid cells (Fig. 4E,F & video
268 10). Chromosome segregation defects can result in aneuploidy and micronuclei formation (Molina
269 et al., 2020). We found a small percentage of hybrid cells containing micronuclei, but more
270 frequently discovered heterokaryons (hybrid cells containing two nuclei of different origin). In
271 most cases, hybrid cells fused both nuclei into one, forming synkaryons (Fig. 4G).
272 Aneuploidy has been proposed to be a hallmark of cancer (Molina et al., 2020) but appears
273 to be context dependent (Ben-David and Amon, 2020). To test whether neuroblast – GMC derived
274 hybrid cells are sufficient to induce tumor formation, we grafted His2A::GFP expressing larval fly
275 brains after successful induction of cell fusion into the abdomen of wild type hosts (Rossi and
276 Gonzalez, 2015) and monitored the host flies for tumor formation and life span changes. As
277 previously reported (Caussinus and Gonzalez, 2005), brat RNAi expressing brains formed visible
278 tumors in host flies by day 30 and caused a reduction in lifespan of the host. However, larval brains
279 without attempted fusions (wild type transplants), attempted but unsuccessful fusions (controlling
280 for the effect of laser ablation), or induced fusion, showed neither tumor growth by day 30 (or
281 after), nor a reduction in lifespan (Fig. 5A,B). We conclude that chromosome segregation is
282 defective in Nb-GMC hybrid cells but insufficient to form visible tumors in otherwise normal and
283 unperturbed larval fly brains.

284 **Discussion**

285 Cell – cell fusion can occur under normal physiological conditions and has been implicated in
286 malignancy (Platt and Cascalho, 2019) but how hybrid cells recognize and separate endogenous
287 and ectopic chromosomes during mitosis is unclear. Here we have shown *in vivo* that Nb-GMC
288 derived hybrid cells separate endogenous chromosomes from the introduced ectopic GMC
289 chromosomes until metaphase and potentially during anaphase. Chromosome separation is
290 achieved through a dual-spindle mechanism; both endogenous and ectopic chromosomes nucleate
291 two independent spindles, most likely through the canonical centrosome pathway. These dual
292 spindles co-align during metaphase, thereby congressing the two chromosome clusters at the
293 metaphase plate. Endogenous and ectopic chromosomes independently segregate during
294 anaphase, manifested in delayed segregation onset of ectopic chromatin. Although chromosome
295 missegregation is frequent in hybrid cells, potentially leading to aneuploidy, we failed to detect
296 malignant tumor formation when hybrid cell – containing larval brains were grafted into wild type
297 host flies.

298 Taken together, we propose that endogenous and ectopic chromosome separation is achieved
299 through an early microtubule-dependent chromosome capture mechanism that retains
300 endogenous chromosomes in close proximity to the apical neuroblast cortex during interphase. In
301 addition to this geometrical separation, the nuclear envelope might impose a physical boundary,
302 preventing random chromosome mixing prior to chromosome congression (Fig. 5C). In pre-mitotic
303 neuroblasts, chromatin can be connected with centrosomes through the Linc complex (Lee and
304 Burke, 2018), potentially implicating the SUN domain protein Klaroid (Kracklauer et al., 2007)
305 and the KASH-domain protein Klarsicht (Razafsky and Hodzic, 2009; Lee and Burke, 2018) in
306 asymmetric chromatin clustering and the prevention of chromatin mixing during interphase.

307 The chromatin separation mechanisms described here could be applicable to chromosome
308 separation occurring in the first cleavage after fertilization in insects, arthropods and vertebrates
309 (Reichmann et al., 2018; Kawamura, 2001). Similarly, biased chromatid segregation has been
310 observed in stem cells (Yadlapalli and Yamashita, 2013; Ranjan et al., 2019) and meiosis (Akera
311 et al., 2017). Since centromeres have also been found to be confined to specific nuclear locations
312 in many organisms (Weierich et al., 2003; Muller et al., 2019), it will be interesting to see whether
313 microtubule-dependent chromatin attachment provides an alternative mechanism for biased sister
314 chromatid segregation or other important cellular functions.
315
316
317

References

Aichel, O. 1911. Über Zellverschmelzung mit quantitativ abnormer Chromosomenverteilung als Ursache der Geschwulstbildung. W. Roux, editor. Verlag von Wilhelm Engelmann.

Akera, T., L. Chmátal, E. Trimm, K. Yang, C. Aonbangkhen, D.M. Chenoweth, C. Janke, R.M. Schultz, and M.A. Lampson. 2017. Spindle asymmetry drives non-Mendelian chromosome segregation. *Science*. 358:668 672. doi:10.1126/science.aan0092.

Akera, T., E. Trimm, and M.A. Lampson. 2019. Molecular Strategies of Meiotic Cheating by Selfish Centromeres. *Cell*. 178:1132-1144.e10. doi:10.1016/j.cell.2019.07.001.

Arco, A.G. del, B.A. Edgar, and S. Erhardt. 2018. In Vivo Analysis of Centromeric Proteins Reveals a Stem Cell-Specific Asymmetry and an Essential Role in Differentiated, Non-proliferating Cells. *Cell Reports*. 22:1982–1993. doi:10.1016/j.celrep.2018.01.079.

Ben-David, U., and A. Amon. 2020. Context is everything: aneuploidy in cancer. *Nat Rev Genet*. 21:44–62. doi:10.1038/s41576-019-0171-x.

Blachon, S., J. Gopalakrishnan, Y. Omori, A. Polyanovsky, A. Church, D. Nicastro, J. Malicki, and T. Avidor-Reiss. 2008. Drosophila asterless and vertebrate Cep152 Are orthologs essential for centriole duplication. *Genetics*. 180:2081 2094. doi:10.1534/genetics.108.095141.

Boveri, T. 2008. Concerning the Origin of Malignant Tumours by Theodor Boveri. Translated and annotated by Henry Harris. *J Cell Sci*. 121:1–84. doi:10.1242/jcs.025742.

Buszczak, M., S. Paterno, D. Lighthouse, J. Bachman, J. Planck, S. Owen, A.D. Skora, T.G. Nystul, B. Ohlstein, A. Allen, J.E. Wilhelm, T.D. Murphy, R.W. Levis, E. Matunis, N. Srivali, R.A. Hoskins, and A.C. Spradling. 2007. The carnegie protein trap library: a versatile tool for Drosophila developmental studies. *Genetics*. 175:1505 1531. doi:10.1534/genetics.106.065961.

Cabernard, C., and C.Q. Doe. 2009. Apical/basal spindle orientation is required for neuroblast homeostasis and neuronal differentiation in Drosophila. *Dev Cell*. 17:134 141. doi:10.1016/j.devcel.2009.06.009.

Cabernard, C., K.E. Prehoda, and C.Q. Doe. 2010. A spindle-independent cleavage furrow positioning pathway. *Nature*. 467:91 94. doi:10.1038/nature09334.

Caussinus, E., and C. Gonzalez. 2005. Induction of tumor growth by altered stem-cell asymmetric division in Drosophila melanogaster. *Nat Genet*. 37:1125 1129. doi:10.1038/ng1632.

Dietzl, G., D. Chen, F. Schnorrer, K.-C. Su, Y. Barinova, M. Fellner, B. Gasser, K. Kinsey, S. Oppel, S. Scheiblauer, A. Couto, V. Marra, K. Keleman, and B.J. Dickson. 2007. A genome-wide transgenic RNAi library for conditional gene inactivation in Drosophila. *Nature*. 448:151 156. doi:10.1038/nature05954.

354 Drpic, D., A.C. Almeida, F. Renda, J. Damas, H.A. Lewin, D.M. Larkin, A. Khodjakov, and H. Maiato.
355 2018. Chromosome Segregation Is Biased by Kinetochore Size. *Curr Biol*. 28:1344 1356.e5.
356 doi:10.1016/j.cub.2018.03.023.

357 Fukagawa, T., and W.C. Earnshaw. 2014. The Centromere: Chromatin Foundation for the Kinetochore
358 Machinery. *Dev Cell*. 30:496–508. doi:10.1016/j.devcel.2014.08.016.

359 Gallaud, E., A.R. Nair, N. Horsley, A. Monnard, P. Singh, T.T. Pham, D.S. Garcia, A. Ferrand, and C.
360 Cabernard. 2020. Dynamic centriolar localization of Polo and Centrobin in early mitosis primes
361 centrosome asymmetry. *Plos Biol*. 18:e3000762. doi:10.1371/journal.pbio.3000762.

362 Gallaud, E., T. Pham, and C. Cabernard. 2017. Drosophila melanogaster Neuroblasts: A Model for
363 Asymmetric Stem Cell Divisions. *Results Problems Cell Differ*. 61:183 210. doi:10.1007/978-3-319-
364 53150-2_8.

365 Gratz, S.J., A.M. Cummings, J.N. Nguyen, D.C. Hamm, L.K. Donohue, M.M. Harrison, J. Wildonger,
366 and K.M. O'Connor-Giles. 2013. Genome Engineering of Drosophila with the CRISPR RNA-Guided
367 Cas9 Nuclease. *Genetics*. 194:1029–1035. doi:10.1534/genetics.113.152710.

368 Heasley, L.R., S.M. Markus, and J.G. DeLuca. 2017. "Wait Anaphase" Signals Are Not Confined to the
369 Mitotic Spindle. *Mol Biol Cell*. 28:1186–1194. doi:10.1091/mbc.e17-01-0036.

370 Henikoff, S., K. Ahmad, J.S. Platero, and B. van Steensel. 2000. Heterochromatic deposition of
371 centromeric histone H3-like proteins. *Proc National Acad Sci*. 97:716–721.
372 doi:10.1073/pnas.97.2.716.

373 Januschke, J., and C. Gonzalez. 2010. The interphase microtubule aster is a determinant of asymmetric
374 division orientation in Drosophila neuroblasts. *J Cell Biology*. 188:693 706.
375 doi:10.1083/jcb.200905024.

376 Januschke, J., S. Llamazares, J. Reina, and C. Gonzalez. 2011. Drosophila neuroblasts retain the daughter
377 centrosome. *Nat Commun*. 2:243. doi:10.1038/ncomms1245.

378 Januschke, J., J. Reina, S. Llamazares, T. Bertran, F. Rossi, J. Roig, and C. Gonzalez. 2013. Centrobin
379 controls mother–daughter centriole asymmetry in Drosophila neuroblasts. *Nat Cell Biol*. 15:241 248.
380 doi:10.1038/ncb2671.

381 Katsani, K.R., R.E. Karess, N. Dostatni, and V. Doye. 2008. In Vivo Dynamics of Drosophila Nuclear
382 Envelope Components. *Mol Biol Cell*. 19:3652–3666. doi:10.1091/mbc.e07-11-1162.

383 Kawamura, N. 2001. Fertilization and the first cleavage mitosis in insects. *Dev Growth Differ*. 43:343–
384 349. doi:10.1046/j.1440-169x.2001.00584.x.

385 Kracklauer, M.P., S.M.L. Banks, X. Xie, Y. Wu, and J.A. Fischer. 2007. Drosophila klaroid Encodes a
386 SUN Domain Protein Required for Klarsicht Localization to the Nuclear Envelope and Nuclear
387 Migration in the Eye. *Fly*. 1:75–85. doi:10.4161/fly.4254.

388 Lee, Y.L., and B. Burke. 2018. LINC complexes and nuclear positioning. *Semin Cell Dev Biol*. 82:67 76.
389 doi:10.1016/j.semcdb.2017.11.008.

390 Maiato, H., A.M. Gomes, F. Sousa, and M. Barisic. 2017. Mechanisms of Chromosome Congression
391 during Mitosis. *Biology*. 6:13. doi:10.3390/biology6010013.

392 McIntosh, J.R. 2016. Mitosis. *Csh Perspect Biol*. 8:a023218. doi:10.1101/cshperspect.a023218.

393 Molina, O., M.A. Abad, F. Solé, and P. Menéndez. 2020. Aneuploidy in Cancer: Lessons from Acute
394 Lymphoblastic Leukemia. *Trends Cancer*. doi:10.1016/j.trecan.2020.08.008.

395 Muller, H., J. Gil, and I.A. Drinnenberg. 2019. The Impact of Centromeres on Spatial Genome
396 Architecture. *Trends Genet*. 35:565–578. doi:10.1016/j.tig.2019.05.003.

397 Musacchio, A. 2015. The Molecular Biology of Spindle Assembly Checkpoint Signaling Dynamics. *Curr*
398 *Biol*. 25:R1002 18. doi:10.1016/j.cub.2015.08.051.

399 Platt, J.L., and M. Cascalho. 2019. Cell Fusion in Malignancy: A Cause or Consequence? A Provocateur
400 or Cure? *Cells*. 8:587. doi:10.3390/cells8060587.

401 Prosser, S.L., and L. Pelletier. 2017. Mitotic spindle assembly in animal cells: a fine balancing act. *Nat*
402 *Rev Mol Cell Bio*. 18:187–201. doi:10.1038/nrm.2016.162.

403 Quintyne, N.J., J.E. Reing, D.R. Hoffelder, S.M. Gollin, and W.S. Saunders. 2005. Spindle Multipolarity
404 Is Prevented by Centrosomal Clustering. *Science*. 307:127–129. doi:10.1126/science.1104905.

405 Ranjan, R., J. Snedeker, and X. Chen. 2019. Asymmetric Centromeres Differentially Coordinate with
406 Mitotic Machinery to Ensure Biased Sister Chromatid Segregation in Germline Stem Cells. *Cell Stem*
407 *Cell*. doi:10.1016/j.stem.2019.08.014.

408 Razafsky, D., and D. Hodzic. 2009. Bringing KASH under the SUN: the many faces of nucleo-
409 cytoskeletal connections. *J Cell Biology*. 186:461 472. doi:10.1083/jcb.200906068.

410 Reichmann, J., B. Nijmeijer, M.J. Hossain, M. Eguren, I. Schneider, A.Z. Politi, M.J. Roberti, L.
411 Hufnagel, T. Hiiragi, and J. Ellenberg. 2018. Dual-spindle formation in zygotes keeps parental
412 genomes apart in early mammalian embryos. *Science*. 361:189 193. doi:10.1126/science.aar7462.

413 Rieder, C.L., A. Khodjakov, L.V. Paliulis, T.M. Fortier, R.W. Cole, and G. Sluder. 1997. Mitosis in
414 vertebrate somatic cells with two spindles: Implications for the metaphase/anaphase transition
415 checkpoint and cleavage. *Proc National Acad Sci*. 94:5107–5112. doi:10.1073/pnas.94.10.5107.

416 Rossi, F., and C. Gonzalez. 2015. Studying tumor growth in Drosophila using the tissue allograft method.
417 *Nat Protoc*. 10:1525–1534. doi:10.1038/nprot.2015.096.

418 Roubinet, C., A. Tsankova, T.T. Pham, A. Monnard, E. Caussinus, M. Affolter, and C. Cabernard. 2017.
419 Spatio-temporally separated cortical flows and spindle geometry establish physical asymmetry in fly
420 neural stem cells. *Nat Commun*. 8:1383. doi:10.1038/s41467-017-01391-w.

421 Sunchu, B., and C. Cabernard. 2020. Principles and mechanisms of asymmetric cell division.
422 *Development*. 147:dev167650. doi:10.1242/dev.167650.

423 Thomas, G.E., M.R. Renjith, and T.K. Manna. 2017. Kinetochore–microtubule interactions in
424 chromosome segregation: lessons from yeast and mammalian cells. *Biochem J*. 474:3559–3577.
425 doi:10.1042/bcj20170518.

426 Weierich, C., A. Brero, S. Stein, J. von Hase, C. Cremer, T. Cremer, and I. Solovei. 2003. Three-
427 dimensional arrangements of centromeres and telomeres in nuclei of human and murine lymphocytes.
428 *Chromosome Res*. 11:485–502. doi:10.1023/a:1025016828544.

429 Yadlapalli, S., and Y.M. Yamashita. 2013. Chromosome-specific nonrandom sister chromatid segregation
430 during stem-cell division. *Nature*. 498:251 254. doi:doi:10.1038/nature12106.

431 Yu, K., N. Zhong, Y. Xiao, and Z. She. 2019. Mechanisms of kinesin-7 CENP-E in kinetochore–
432 microtubule capture and chromosome alignment during cell division. *Biol Cell*. 111:143–160.
433 doi:10.1111/boc.201800082.

434
435

436 **Figures**

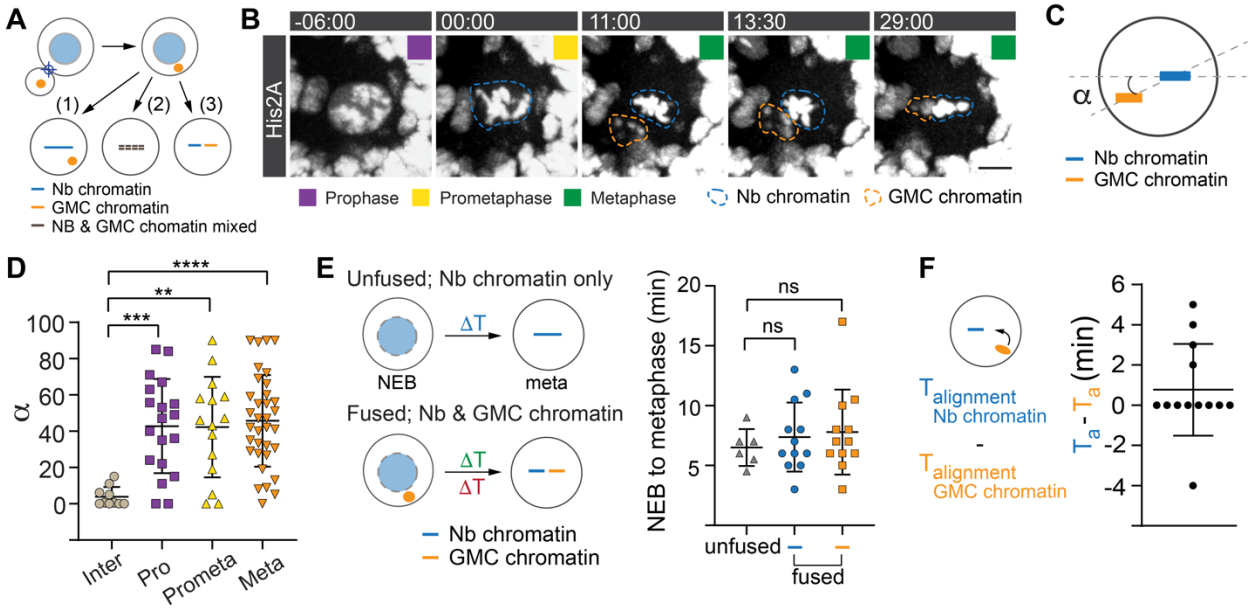

437

438

439 **Figure 1: Nb-GMC hybrid cells align Nb and GMC chromatin independently at the**
440 **metaphase plate.**

441 (A) Nb – GMC derived hybrid cells could (1) only align neuroblast chromosomes at the metaphase
442 plate, (2) congress a mix of endogenous and ectopic chromosomes or (3) separately align Nb and
443 GMC chromosomes at the metaphase plate. (B) Representative image sequence of a dividing third
444 instar larval neuroblast Nb-GMC hybrid cell, expressing the histone marker His2A::GFP (dashed
445 blue circle: endogenous chromatin; dashed orange circle: ectopic chromatin). (C) Alignment of
446 endogenous and ectopic chromatin in hybrid cells derived from interphase (inter), prophase (pro),
447 prometaphase (prometa) or metaphase (meta) fusions were quantified with angle measurements
448 in metaphase and plotted in (D). (E) Chromosome alignment time for endogenous (blue spheres)
449 and ectopic chromosomes (orange squares) compared to unfused control neuroblasts (grey
450 triangles) Colored boxes represent corresponding cell cycle stages. One-way ANOVA was used for
451 (D) and (E). Error bars correspond to standard deviation (SD). * $p<0.05$, **$p<0.01$,****
452 $p<0.000.1$. For this and subsequent Figures, exact p values and complete statistical information
453 can be found in Supplemental table 1. Time in mins:secs. Scale bar is 5 μm.

454

455

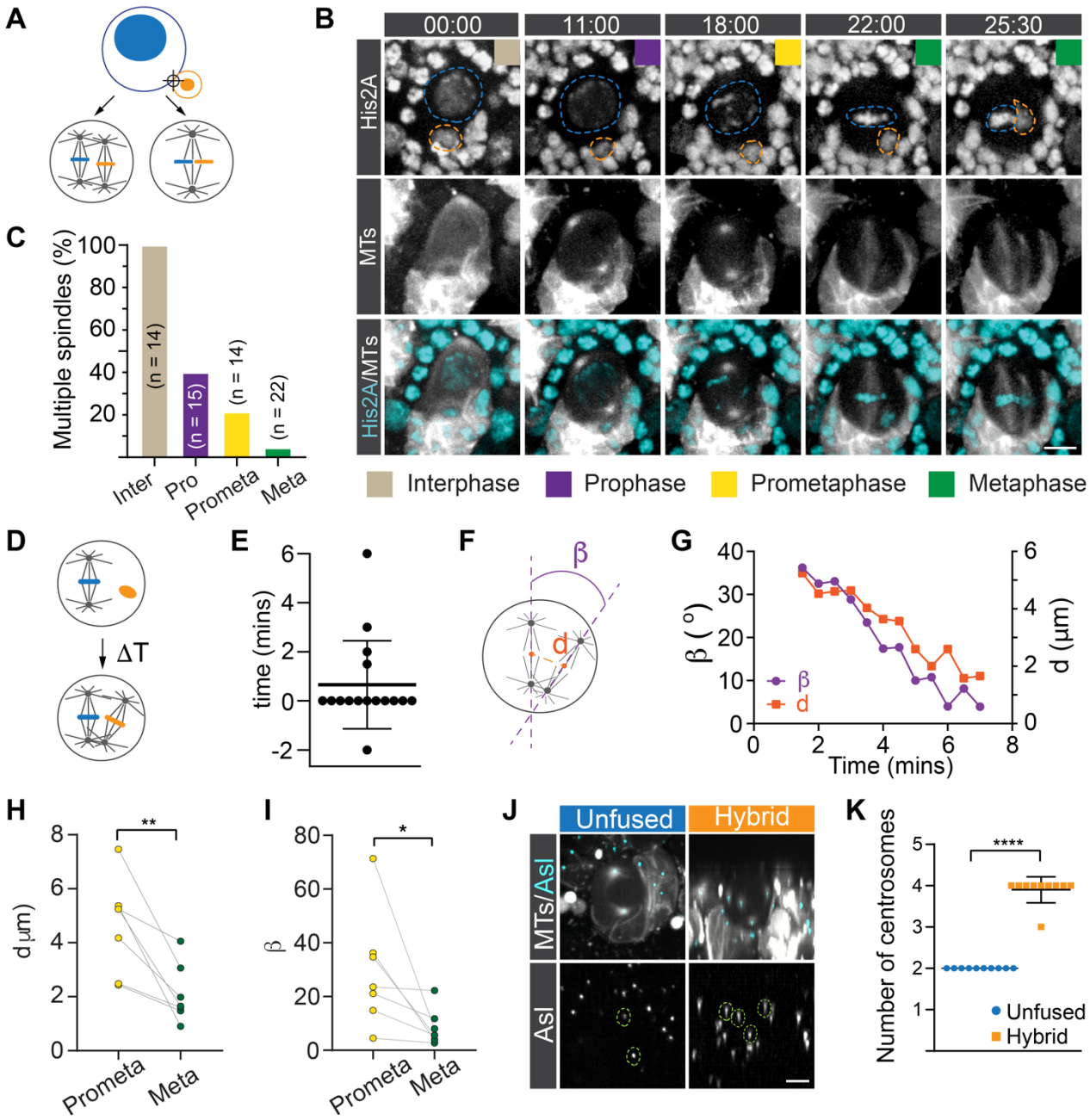

Figure 2: Dual spindles align endogenous and ectopic spindles separately at the metaphase plate.

(A) Nb – GMC derived hybrid cells could align neuroblast and GMC chromosomes either through a single or dual-spindle mechanism. (B) Representative third instar larval Nb-GMC hybrid cell, expressing the histone marker His2A::GFP (white in top row; cyan in merged channel below), the MT marker cherry::Jupiter (white in middle and bottom row). (C) Quantification of hybrid cells containing dual- or multiple spindles for hybrid cells derived from interphase (inter), prophase

464 (pro), prometaphase (prometa) or metaphase (meta) fusions. (D) The time difference between
465 endogenous and ectopic spindle formation was measured in hybrid cells and plotted in (E). (F)
466 Spindle angle and inter-spindle distances were measured during mitosis. A representative example
467 is shown in (G). Quantification of inter-spindle (H) distances and (I) angles at prometaphase and
468 metaphase. (J) A representative third instar larval Nb-GMC hybrid, expressing the centriole
469 marker, Asl::GFP (cyan; top row. White; bottom row) and the spindle marker cherry::Jupiter (MTs;
470 white in top row). Centrosomes were highlighted with green dashed circles. (K) Comparison of
471 centrosome number between unfused wild type and hybrid cells.
472 Colored boxes represent corresponding cell cycle stages. Error bars correspond to SDs. Figures (H)
473 and (I) paired t-test, Figures (K) unpaired t-test. * $p<0.05$, ** $p<0.01$, **** $p<0.000$. Time in
474 mins:secs. Scale bar is 5 μm.
475
476

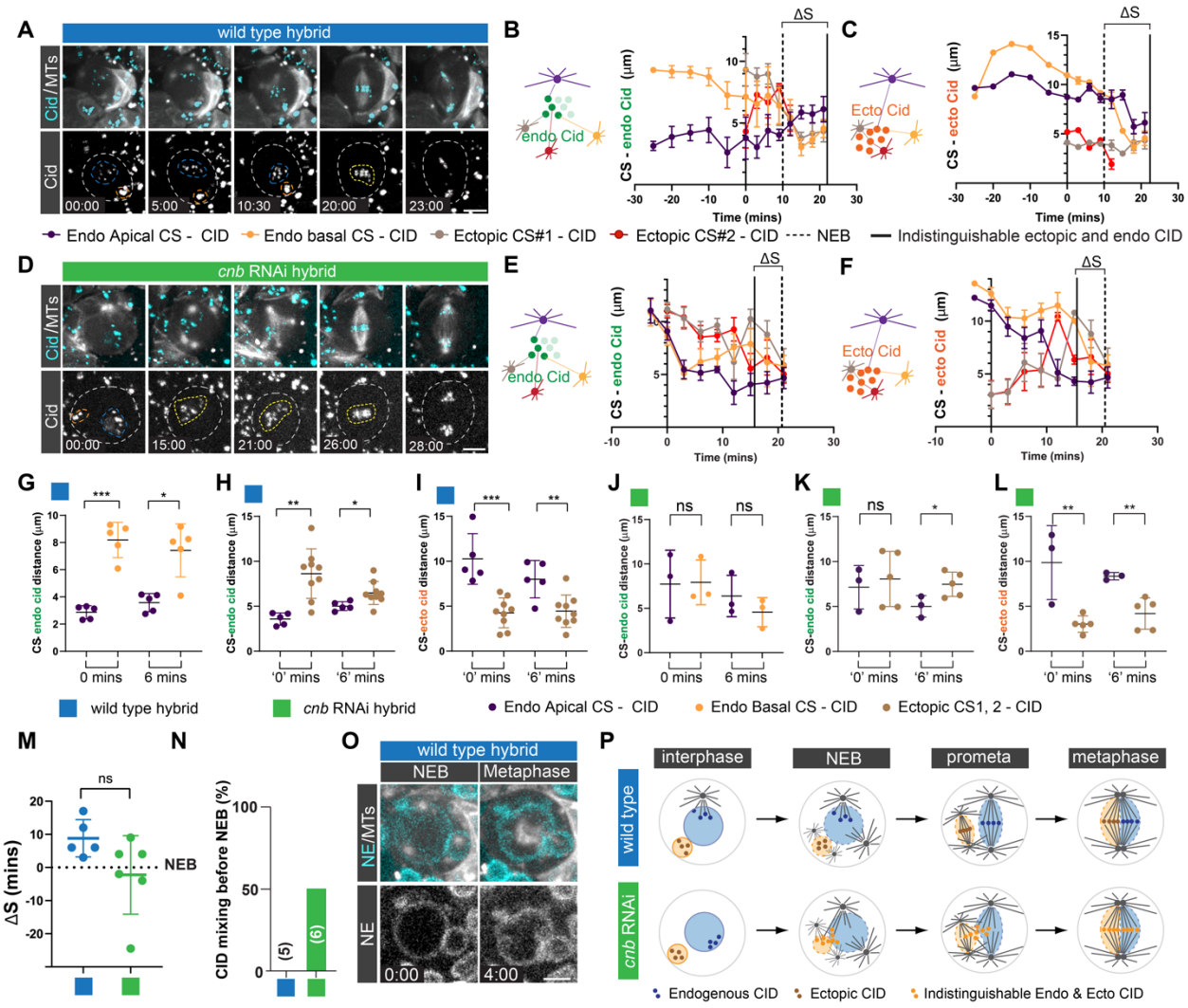

Figure 3: Asymmetric microtubule dependent centrosome-chromatin attachments contribute to the separation of endogenous and ectopic chromosomes.

Representative third instar larval (A) wild type or (D) *cnb* RNAi expressing Nb-GMC hybrid cell, expressing Cid::EGFP (top row; cyan, bottom row; white) and the microtubule marker cherry::Jupiter (white; top row). Neuroblast-derived and GMC-derived Cid clusters are outlined with a blue and orange dashed line, respectively. The white dashed line labels the cell outline. Indistinguishable GMC and Nb Cid clusters are highlighted with yellow dashed circles. The distance of (B) endogenous or (C) ectopic Cid from the wild type hybrid cell shown in (A) in relation to GMC and Nb centrosomes plotted over time. (E) Endogenous or (F) ectopic Cid – centrosome distance measurements of the cnb RNAi expressing hybrid cell shown in (D). The vertical solid line indicates the time point when endogenous and ectopic Cid can no longer be distinguished. Vertical

490 dashed line indicates nuclear envelope breakdown. Measurements of endogenous Cid – apical
491 (purple) or basal (yellow) endogenous centrosomes were plotted when (G) the endogenous basal
492 centrosome matured (0 mins) and 6 minutes thereafter (6mins) or (H) the ectopic centrosomes
493 matured ('0' mins) and 6 minutes thereafter. Corresponding measurements of *cnb* RNAi expressing
494 hybrid cells are shown in (J) and (K). Distance of ectopic Cid in relation to endogenous and ectopic
495 centrosomes shown for (I) wild type or (L) *cnb* RNAi expressing hybrid cells. (M) Time interval
496 between NEB and mixing of endogenous and ectopic Cid for wild type (blue circles) and *cnb* RNAi
497 expressing (green circles) hybrid cells. (N) Bar graph showing percentage of hybrid cells in which
498 the endogenous and ectopic CID mixed prior to NEB. (O) A third instar wild type hybrid cell
499 expressing the nuclear envelope (NE) marker, koi::GFP (cyan; top row, white; bottom row) and
500 cherry::Jupiter. (P) Schematic summary: separation of endogenous and ectopic chromosomes
501 depends on microtubule dependent, asymmetric chromatin-centrosome attachments and physical
502 separation through nuclear envelopes. *cnb* RNAi expressing neuroblasts release endogenous Cid
503 during interphase, partially randomizing re-attachment in the subsequent mitosis, which causes
504 premature mixing of endogenous and ectopic Cid. Colored boxes refer to the indicated cell cycle
505 stages. Error bars correspond to SDs. Figure (G) paired t-test and Figures (H-L) unpaired t-test. ns
506 – no signficiance, * $p<0.05$, ** $p<0.01$, *** $p<0.0001$, **** $p<0.0001$. Time in mins:secs. Scale
507 bar is 5 μm.
508

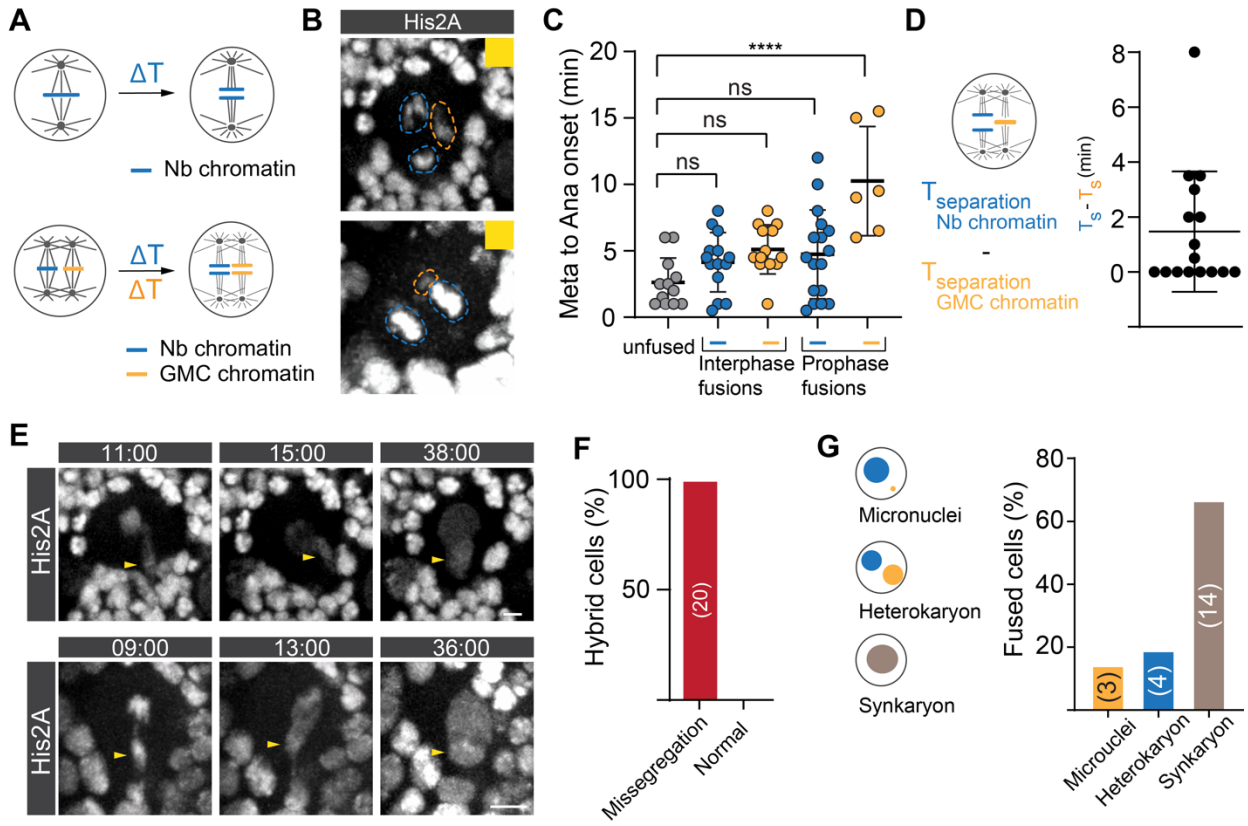

Figure 4: Ectopic chromosomes in hybrid cells segregate independently but erroneously. (A) The time between chromosome alignment (metaphase) and separation (anaphase onset) was measured for endogenous and ectopic chromosomes in wild type hybrid cells and plotted in (C). (B) Representative examples of delayed (top row) and simultaneous (bottom row) segregation of endogenous (blue dashed circle) and ectopic (orange dashed circle) chromosomes in wild type hybrid cells expressing the chromatin marker His2A::GFP. (C) Quantification of metaphase to anaphase onset in control Nbs, compared to interphase and prophase Nb-GMC hybrids. (D) Average time difference between Nb and GMC chromatin anaphase onset in Nb-GMC hybrid cells. (E) Two representative third instar larval Nb-GMC hybrids expressing histone marker His2A::GFP showing missegregating chromatids (yellow arrows) during anaphase. Time stamps are in relation to NEB (=0:00). (F) Bar graph showing percentage of Nb-GMC hybrid cells with missegregating chromatids. (G) Bar graph quantifying the percentage of fused cells with micronuclei, heterokaryons or synkaryons. ΔT; time difference. Error bars correspond to SDs. One way ANOVA test was used in (C). ns – no significance, **** $p<0.0001$. Time in mins:secs. Scale bar is 5 μm.

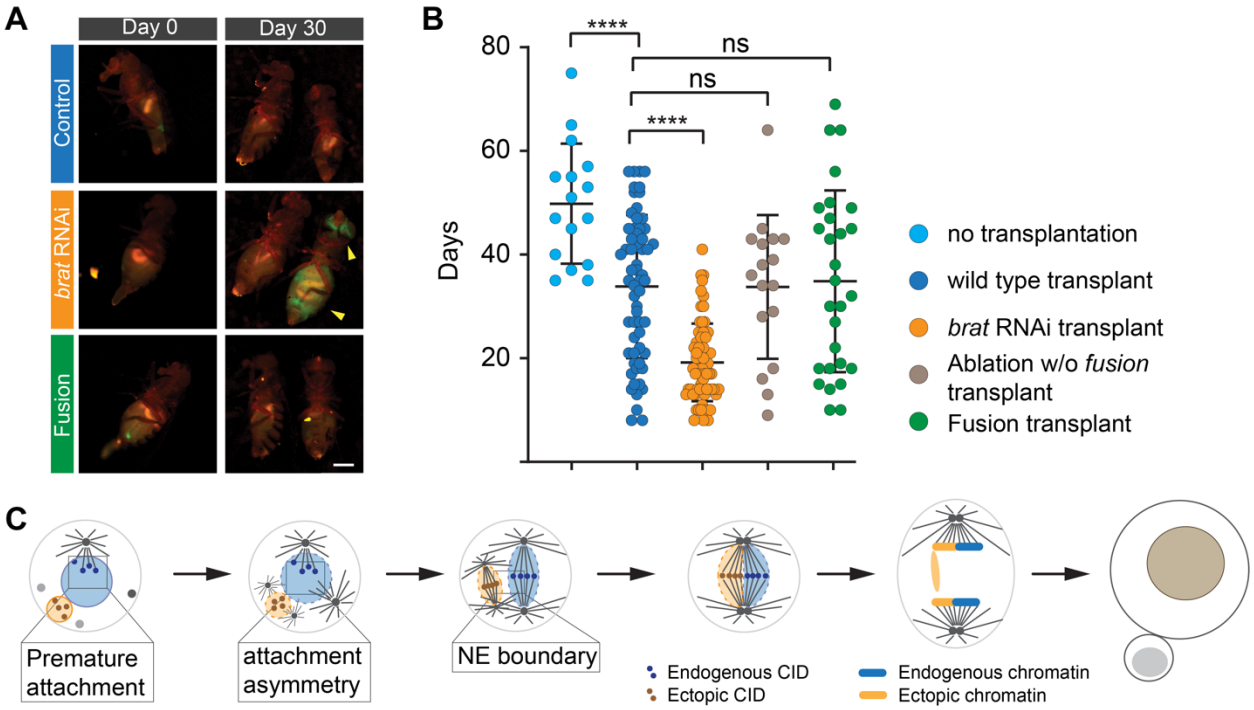

Figure 5: Nb – GMC derived hybrid cells neither form visible tumors nor reduce the lifespan in adult hosts.

(A) Third instar larval brains expressing His2A::GFP (top row; negative control), co-expressing *brat* RNAi (middle row; positive control) or containing Nb – GMC hybrid cells (bottom row) were transplanted into wild type hosts and imaged at the day of transplantation (day 0) and Day 30. Yellow arrowheads highlight tumors in wild type hosts transplanted with brat RNAi expressing brains. (B) Scatter plot showing the lifespan of host flies after brain grafts. Grafted tissue either contained no fusions (wild type transplants), expressing *brat* RNAi without fusions (brat RNAi transplants), attempted but unsuccessful fusion (ablation without fusion transplants) and with brains containing hybrid cells (fusion transplants). Host flies without transplanted tissue were plotted for comparison (no transplantation). Error bars correspond to SDs. One way ANOVA. ns – no signficiance, **, ****$p<0.0001$. Scale bar, 1000 μm. (C) Model: Asymmetric MTOCs capture neuroblast chromatin during interphase, thereby establishing a first physical separation between endogenous and ectopic chromatin. Nuclear envelopes form an additional physical barrier. As hybrid cells enter mitosis, the neuroblast centrosomes and introduced ectopic GMC centrosomes nucleate two separate bipolar spindles, aligning their respective chromatin at the metaphase plate. This separation persists through anaphase. Ectopic chromosomes fail to segregate accurately.

544 **Supplemental Data**
545
546

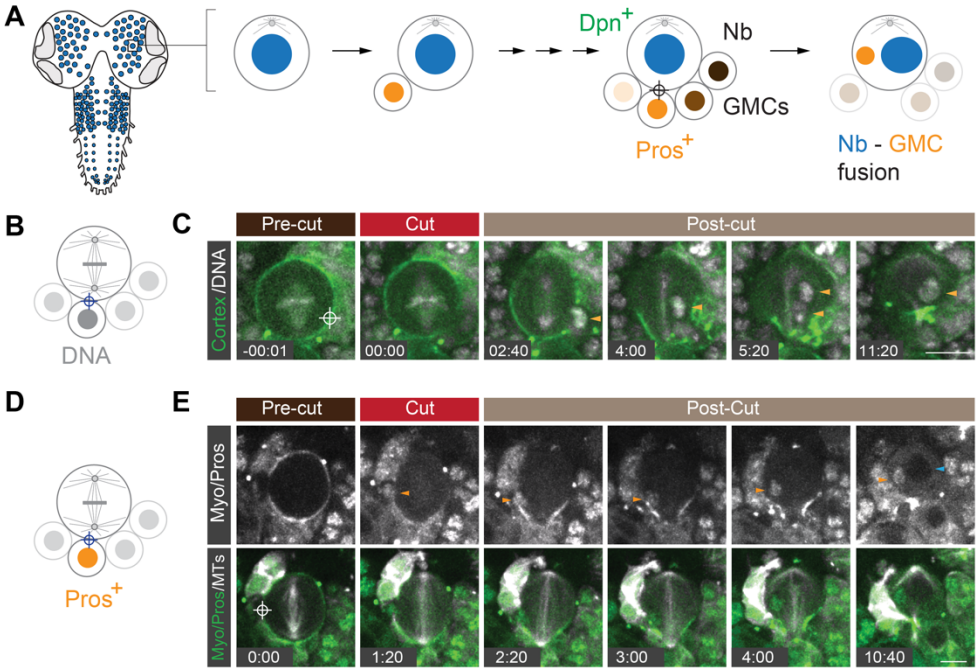

547
548

549 **Fig.S1: Acute induced Nb – GMC fusion in Drosophila larval brains.**

550 (A) Schematic representation of a third instar *Drosophila* larval brain and neural stem cell division
551 mode. Neural stem cells (neuroblasts (Nbs); blue circles) divide asymmetrically, generating a
552 Prospero-positive, differentiating ganglion mother cell (GMC; Pros+) while self-renewing the
553 Dpn^+ neuroblast. GMCs cluster around Nbs and can be identified based on size and Prospero
554 expression. Acute Nb – GMC fusion can result in hybrid cells containing two molecularly distinct
555 nuclei. (B) Experimental outline and (C) representative example of a metaphase wild type
556 neuroblast, expressing the cell cortex marker Sqh::EGFP (green), the mitotic spindle marker
557 cherry::Jupiter (white) and the chromatin marker His2A::RFP (white). The site targeted by the
558 ablation laser is highlighted with the white crosshair. The orange arrowhead labels a GMC nucleus
559 moving into the Nb. This hybrid cell successfully completes cytokinesis. (D) Schematic and (E)
560 representative example of a wild type early anaphase neuroblast expressing Sqh::EGFP (white;
561 top, green; bottom), cherry::Jupiter (white) and Pros::EGFP (white). The orange arrowhead
562 highlights a $Pros^+$ GMC nucleus moving into the neuroblast. Cytokinesis completes, creating a
563 hybrid cell containing a $Pros^+$ and $Pros^-$ nucleus. Time in min:sec; scale bar: 10μm.
564

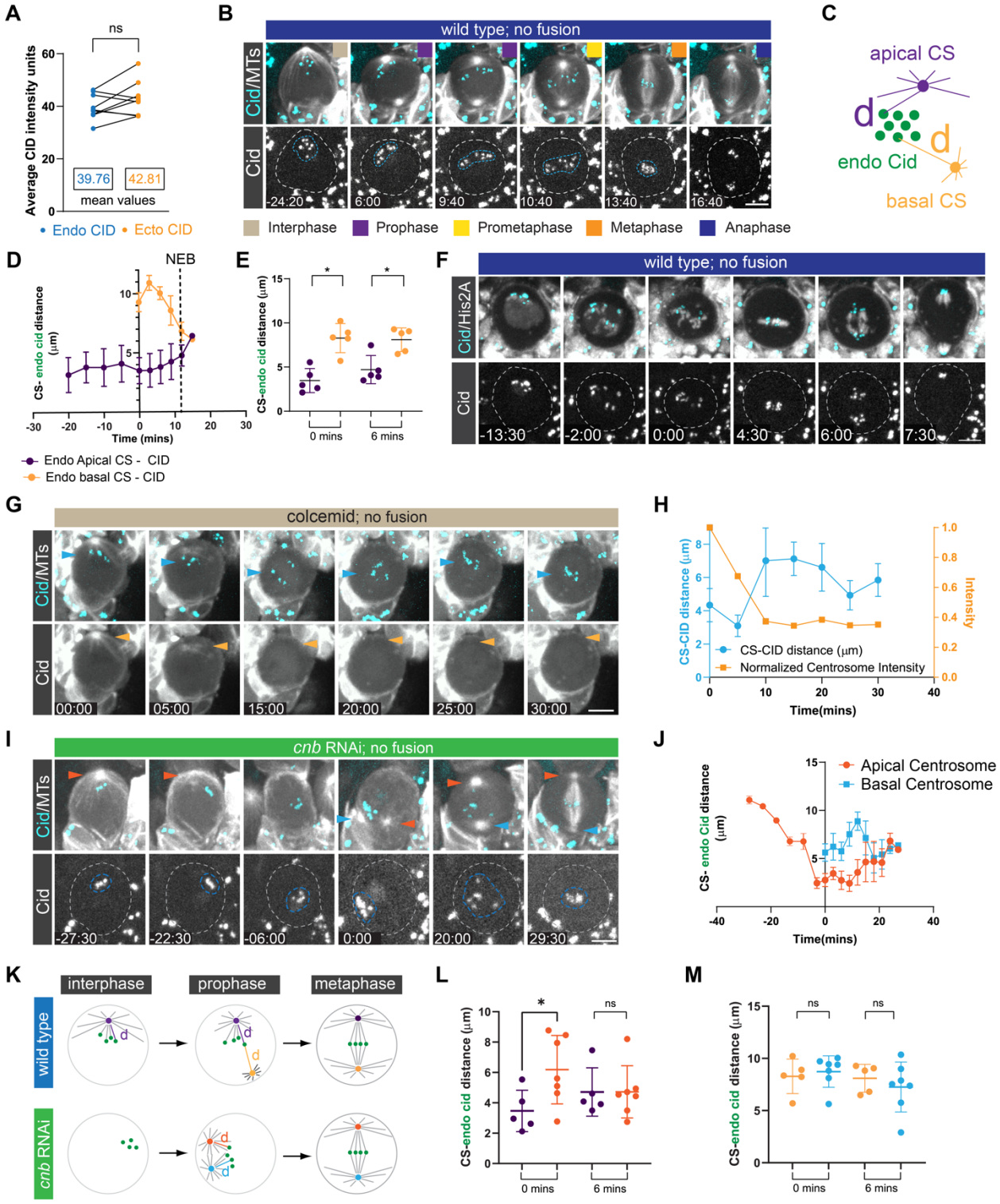
A
ns
Average CID intensity units
39.76
42.81
mean values
Endo CID
Ecto CID
B
wild type; no fusion
Cid/MTs
Cid
-24:20
6:00
9:40
10:40
13:40
16:40
Interphase
Prophase
Prometaphase
Metaphase
Anaphase
C
apical CS
d
d
endo Cid
basal CS
D
NEB
CS- endo cid distance (µm)
Time (mins)
Endo Apical CS - CID
Endo basal CS - CID
E
CS-endo cid distance (µm)
0 mins
6 mins
F
wild type; no fusion
Cid/His2A
Cid
-13:30
-2:00
0:00
4:30
6:00
7:30
G
colcemid; no fusion
Cid/MTs
Cid
00:00
05:00
15:00
20:00
25:00
30:00
H
CS-CID distance (µm)
Intensity
CS-CID distance (µm)
Normalized Centrosome Intensity
Time(mins)
I
cnb RNAi; no fusion
Cid/MTs
Cid
-27:30
-22:30
-06:00
0:00
20:00
29:30
J
Apical Centrosome
Basal Centrosome
CS- endo Cid distance (µm)
Time(mins)
K
interphase
prophase
metaphase
wild type
cnb RNAi
L
CS-endo cid distance (µm)
0 mins
6 mins
Wild Type; Apical CS
Cnb RNAi; Apical CS
M
CS-endo cid distance (µm)
0 mins
6 mins
Wild Type; Basal CS
Cnb RNAi; Basal CS

565

566

567

Fig.S2: Microtubule-dependent, asymmetric chromatin-centrosome attachments retain chromosomes close to the apical neuroblast cortex during interphase.

(A) CID intensity measurements of endogenous and ectopic CID in Nb-GMC hybrid cells (p-value, 0.1294). (B) Representative third instar larval neuroblast expressing the centromere specific histone-3 variant marker, Cid::EGFP (cyan; top, white; bottom) and the microtubule marker cherry::Jupiter. Colored boxes represent corresponding cell cycle stages. (C) The distance between the apical (purple) and basal centrosome (yellow) and individual Cid clusters (green circles), were measured throughout the cell cycle and plotted in (D). Centrosome – Cid distance of an unperturbed wild type neuroblast at the time of basal centrosome maturation (0 mins) and 6 mins thereafter. (F) Representative wild type neuroblast expressing the canonical histone marker His2A::GFP (white) and Cid::EGFP (cyan; top, white; below). The white dashed line highlights the cell outline. (G) Representative example of a wild type neuroblast expressing Cid::EGFP (cyan) and the microtubule marker cherry::Jupiter treated with colcemid. Blue and yellow arrowheads highlight the position of Cid clusters and the disappearing apical MTOC, respectively. (H) MTOC intensity and Cid location measurements for the cell shown in (G). (I) Representative third instar larval neuroblast expressing *cnb* RNAi, cherry::Jupiter (white; top) and Cid::EGFP (cyan; top, white; bottom row). Red arrowheads highlight the disappearing apical MTOC. Blue arrowheads highlight the maturing basal MTOC. Blue dashed circle highlight Cid clusters. The white dashed line highlights the cell outline. (J) Cid – centrosome distance measurement for the cell shown in (I). 'Apical' centrosome refers to the centrosome destined to be positioned on the apical cortex, whereas 'basal' centrosome will be inherited by the basal GMC. (K) Wild type neuroblasts maintain apical CS – Cid attachments in prophase, due to asymmetric MTOC activity and microtubule dependent interphase centrosome – Cid attachments. Cnb RNAi expressing neuroblasts lose MTOC activity in interphase, randomizing the position of Cid clusters. When centrosomes mature again in prophase, both centrosomes simultaneously attach to Cid clusters. (L, M) Cid – centrosome distance measurement in *cnb* RNAi expressing neuroblasts. Error bars correspond to SDs. Fig. (A,E,L,M) -paired t-test. ns – no signficiance, * $p<0.05$. Time in mins:secs. Scale bar is 5 μm.

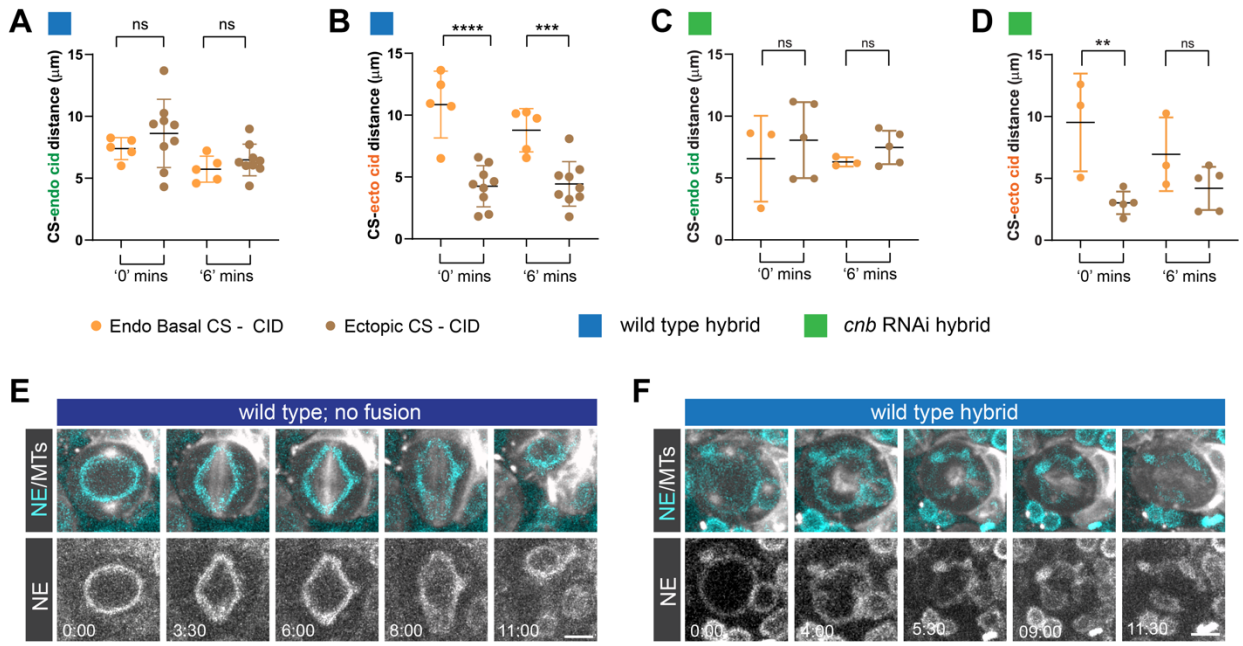

Fig.S3: Asymmetric MTOCs and nuclear envelopes separate endogenous and ectopic chromatin in Nb – GMC hybrid cells.

(A) Averaged distance of basal centrosomes to *endogenous* Cid in wild type or (C) *cnb* RNAi expressing neuroblasts. (B) Averaged distance of basal centrosomes to *ectopic* Cid in wild type or (D) *cnb* RNAi expressing neuroblasts. Measurements are plotted for 0 mins (ectopic centrosome maturation for wild type; ectopic centrosome maturation in cnb RNAi) and 6 mins. Representative image sequence of a wild type (E) unfused neuroblasts or (F) hybrid cell, expressing the nuclear envelope marker koi::GFP (cyan; top, white; bottom) and the microtubule marker cherry::Jupiter (white; top). Error bars correspond to SDs. Fig. (A-D) unpaired t-test. ns – no signficiance, ** $p<0.01$, ***$p<0.001$, ****$p<0.0001$. Time in mins:secs. Scale bar is 5 μm.

Supplemental Table 1: Statistical information

Complete statistical information for the data shown in the corresponding Figures.

614 **Methods**

615

616 **Fly Strains:**

617 Transgenes and fluorescent markers: *worGal4, UAS-mCherry::Jupiter* (Cabernard and Doe, 2009);
618 *worGal4, UAS-mCherry::Jupiter, Sqh::GFP* (Cabernard et al., 2010); *His2A::GFP* (Bloomington
619 stock center); *UAS-mCherry::CAAX, UAS-iLID::CAAX:;mCherry (A. Monnard & C. Cabernard;*
620 *unpublised)*; Cid::EGFP (Ranjan et al., 2019); *pUbq-Asl::GFP* (Blachon et al., 2008); *worgal4, UAS-*
621 *mCherry::Jupiter, Asl::GFP* (this work); *pros::EGFP* (endogenously tagged with CRISPR; this
622 work); *koi::GFP (CB04483)* (Buszczak et al., 2007), *cnb*^{GD11735} RNAi line (v28651) (Dietzl et al.,
623 2007).

624

625 **Generation of pros::EGFP with CRISPR:**

626 Target specific sequences with high efficiency were chosen using the CRISPR Optimal Target
627 Finder (http://tools.flycrispr.molbio.wisc.edu/targetFinder/), the DRSC CRISPR finder
628 (http://www.flyrnai.org/crispr/), and the Efficiency Predictor (http://
629 www.flyrnai.org/evaluateCrispr/) web tools. Sense and antisense primers for these chosen sites
630 were then cloned into pU6-BbsI-ChiRNA (Gratz et al., 2013) between BbsI sites. To generate the
631 replacement donor template, EGFP and 1 kb homology arms flanking the insertion site were cloned
632 into pHD-DsRed-attP (Addgene plasmid #51019) using Infusion technology (Takara/Clontech).
633 Injections were performed in house. Successful events were detected by DsRed-positive screening
634 in the F1 generation. Constitutively active Cre (BDSC#851) was then crossed in to remove the
635 DsRed marker. Positive events were then balanced, genotyped, and sequenced.

636

637

638 **Live cell imaging acute cell-cell fusion:**

639 Imaging medium consists of Schneider's insect medium (Sigma-Aldrich S0146) mixed with 10%
640 BGS (HyClone). Third instar larvae were dissected in imaging medium and the brains were
641 transferred into a μ-slide Angiogenesis or μ-slide 8 well (Ibidi). Live samples were imaged with an
642 Intelligent Imaging Innovations (3i) spinning disc confocal system, consisting of a Yokogawa CSU-
643 W1 spinning disc unit and two Prime 95B Scientific CMOS cameras. A 60x/1.4NA oil immersion
644 objective mounted on a Nikon Eclipse Ti microscope was used for imaging. Live imaging voxels
645 are 0.22 X 0.22 X 0.75-1μm (60x/1.4NA spinning disc).

646 Neuroblast-GMC fusions were induced using a 3i Ablate! ablation system, consisting of a 532nm
647 pulsed laser. We used a pulse width of 7 ns, targeting the membrane interface between the
648 neuroblast and the adjacent GMC.

649

650 **Colcemid treatment:**

651 Dissected brains were incubated with Colcemid (Sigma) in live imaging medium at a final
652 concentration of of 25 μgmL^{-1}.

653

654 **Transplantation experiments:**

655 Brain lobes containing the hybrid cells expressing *His2A::GFP* and *worGal4, UAS-mCherry::Jupiter*
656 were transplanted into 3 to 4 day old, well fed adult w^{1118} female host flies as described previously
657 (Rossi and Gonzalez, 2015). Custom made needles were prepared from Narishige GD-1 glass
658 capillaries using a Narishige, needle puller. Injection needles were shaped with forceps to have a
659 smooth, 45° opening. Transplanted flies were transferred into fresh vials each day for the first three
660 days, followed by biweekly flipping. The tumor growth was monitored and recorded with a Leica
661 MZ FLIII fluorescence stereomicroscope.

Image processing and measurements:

Live cell images were processed using imaris x64 8.3.1 and image J.

For angle and distance measurements, the coordinates for the two spindle poles were determined in Imaris. From these coordinates, angles and distances between spindles were derived based on the calculations outlined below.

Angle between spindles: $\theta = \cos^{-1}\frac{n \cdot \mathrm{e}}{|n||\mathrm{e}|}$

Dot product: $n \cdot \mathrm{e} = (X1*X2) + (Y1*Y2) + (Z1*Z2)$

Magnitude of vectors: $|\mathrm{n}| = \sqrt{X_1^2 + Y_1^2 + z_1^2}$ $|\mathrm{e}| = \sqrt{X_2^2 + Y_2^2 + z_2^2}$

Where **n** corresponds to the spindle vector: **n** (x1,y1,z1) = (N1-N1', N2-N2', N3-N3') and **e** to the ectopic spindle vector: **e** (x2,y2,z2) = (E1-E1', E2-E2', E3-E3')

N1, N2, N3 and N1', N2' and N3' are coordinates of the two poles of the Nb spindle. Similarly, E1, E2, and E3 and E1', E2' and E3' are coordinates of the ectopic spindle poles.

Distance between spindle vectors:

The midpoints of the two spindle vectors are calculated from coordinates of the poles on either side of the respective spindle. This is followed by calculating the distance between these midpoints.

Midpoint of the Nb spindle vector $= \left(\frac{N_1+N_1^1}{2}, \frac{N_2+N_2^1}{2}, \frac{N_3+N_3^1}{2}\right) = (\mathrm{M}_1, \mathrm{M}_2, \mathrm{M}_3)$

Midpoint of the GMC spindle vector $= \left(\frac{G_1+G_1^1}{2}, \frac{G_2+G_2^1}{2}, \frac{G_3+G_3^1}{2}\right) = (m_1, m_2, m_3)$

Distance between these two points $= \sqrt{(\mathrm{M}_1 - \mathrm{m}_1)^2 + (\mathrm{M}_2 - \mathrm{m}_2)^2 + (\mathrm{M}_3 - \mathrm{m}_3)^2}$

Centrosome - Cid distance:

The centrosome (CS) - Cid distance was calculated using Cid and CS coordinates.

CS – Cid distance: $= \sqrt{(\mathrm{x}_1 - \mathrm{x}_2)^2 + (\mathrm{y}_1 - \mathrm{y}_2)^2 + (\mathrm{z}_1 - \mathrm{z}_2)^2}$

Where x_1,y_1,z_1 correspond to CS and x_2,y_2,z_2 to Cid coordinates, respectively.

686 Plotted values correspond to averaged values of all CS – Cid punctae distances and the
687 corresponding standard deviations.
688 0 and 6 mins corresponds to the appearance of the basal centrosome and 6 minutes thereafter.
689 '0' mins and '6' mins corresponds to the appearance of the ectopic centrosome appearance and 6
690 minutes thereafter.
691
692 **Statistical analysis:**
693 Statistical analysis was performed using Graphpad prism 8. Statistical significance was determined
694 using paired or unpaired t-test and one-way ANOVA. Significance was indicated as following: *;
695 $p<0.05$, **;$p<0.01$, ***;$p<0.001$,****$p<0.0001$, ns; not significant. Exact p values and complete
696 statistical information can be found in Extended data table 1.
697
698 **Methods references**
699

700 Blachon, S., J. Gopalakrishnan, Y. Omori, A. Polyanovsky, A. Church, D. Nicastro, J. Malicki,
701 and T. Avidor-Reiss. 2008. Drosophila asterless and vertebrate Cep152 Are orthologs
702 essential for centriole duplication. *Genetics*. 180:2081 2094.
703 doi:10.1534/genetics.108.095141.

704 Buszczak, M., S. Paterno, D. Lighthouse, J. Bachman, J. Planck, S. Owen, A.D. Skora, T.G.
705 Nystul, B. Ohlstein, A. Allen, J.E. Wilhelm, T.D. Murphy, R.W. Levis, E. Matunis, N.
706 Srivali, R.A. Hoskins, and A.C. Spradling. 2007. The carnegie protein trap library: a versatile
707 tool for Drosophila developmental studies. *Genetics*. 175:1505 1531.
708 doi:10.1534/genetics.106.065961.

709 Cabernard, C., and C.Q. Doe. 2009. Apical/basal spindle orientation is required for neuroblast
710 homeostasis and neuronal differentiation in Drosophila. *Dev Cell*. 17:134 141.
711 doi:10.1016/j.devcel.2009.06.009.

712 Cabernard, C., K.E. Prehoda, and C.Q. Doe. 2010. A spindle-independent cleavage furrow
713 positioning pathway. *Nature*. 467:91 94. doi:10.1038/nature09334.

714 Dietzl, G., D. Chen, F. Schnorrer, K.-C. Su, Y. Barinova, M. Fellner, B. Gasser, K. Kinsey, S.
715 Oppel, S. Scheiblauer, A. Couto, V. Marra, K. Keleman, and B.J. Dickson. 2007. A genome-
716 wide transgenic RNAi library for conditional gene inactivation in Drosophila. *Nature*.
717 448:151 156. doi:10.1038/nature05954.

718 Gratz, S.J., A.M. Cummings, J.N. Nguyen, D.C. Hamm, L.K. Donohue, M.M. Harrison, J.
719 Wildonger, and K.M. O'Connor-Giles. 2013. Genome Engineering of Drosophila with the
720 CRISPR RNA-Guided Cas9 Nuclease. *Genetics*. 194:1029–1035.
721 doi:10.1534/genetics.113.152710.

722 Ranjan, R., J. Snedeker, and X. Chen. 2019. Asymmetric Centromeres Differentially Coordinate
723 with Mitotic Machinery to Ensure Biased Sister Chromatid Segregation in Germline Stem
724 Cells. *Cell Stem Cell*. doi:10.1016/j.stem.2019.08.014.

725 Rossi, F., and C. Gonzalez. 2015. Studying tumor growth in Drosophila using the tissue allograft
726 method. *Nat Protoc*. 10:1525–1534. doi:10.1038/nprot.2015.096.

727
728

Acknowledgements

We thank Xin Chen for fly stocks, David Salvador Garcia for generating the Pros::EGFP transgenic line, Sue Biggins and members of the Cabernard laboratory for helpful discussions and comments. This work was supported by the National Institutes of Health (1R01GM126029-03) and a Research Scholar grant from the American Cancer Society (130285-RSG-16253-01-CSM). Stocks obtained from the Bloomington Drosophila Stock Center (NIH P40OD018537) and from the Vienna Drosophila Resource Center (VDRC).

Author contributions

This study was conceived by B.S., N.L. and C.C. B.S and N.L performed all the experiments with significant help from C.S.

B.S, N.L., C.S., and C.C analyzed the data. B.S and C.C. wrote the manuscript.

Competing interest declaration

The authors declare no competing financial interests.

Additional information

This paper contains three Fig. Ss, a supplementary table and 10 videos to support the main conclusions.

751 **Video legends**

752

753 **Video 1: Wild type neuroblast division; related to Fig. 1B**

754 Wild type control (unfused) neuroblast expressing the microtubule binding protein Cherry::Jupiter
755 (white) and the canonical Histone marker His2A::GFP (cyan). Time scale is h:mm:ss and the scale
756 bar is 5 µm

757

758 **Video 2: Wild type hybrid cell; related to Fig. 1B**

759 Wild type hybrid cell derived from a neuroblast – GMC fusion *in vivo*, expressing the canonical
760 Histone marker His2A::GFP (white in single channel; cyan in merge) and the microtubule binding
761 protein Cherry::Jupiter (white). The blue and orange arrows mark endogenous and ectopic
762 chromatin, respectively. Time scale is h:mm:ss and the scale bar is 3 µm.

763

764 **Video 3: Wild type hybrid cell; related to Fig. 2B**

765 Wild type hybrid cell derived from a neuroblast – GMC fusion *in vivo*, expressing the canonical
766 Histone marker His2A::GFP (white in single channel; cyan in merge) and the microtubule binding
767 protein Cherry::Jupiter (white). The blue and orange arrows mark endogenous and ectopic
768 chromatin, respectively. Time scale is h:mm:ss and the scale bar is 2 µm.

769

770 **Video 4: Wild type neuroblast division; related to Fig. S2B**

771 Wild type control (unfused) neuroblast, expressing the microtubule binding protein
772 Cherry::Jupiter (white) and the centromere-specific H3 variant Cid::EGFP (Cyan). Purple and
773 yellow arrows point to the apical and basal centrosome, respectively. The blue arrow refers to
774 moving Cid clusters. Time scale is h:mm:ss and the scale bar is 1 µm.

775 **Video 5: Wild type neuroblast division; related to Fig. S2F**

776 Wild type control (unfused) neuroblast, expressing the membrane marker mCherry::CAAX
777 (white), the canonical Histone marker His2A::GFP (white) and Cid::EGFP (Cyan). The green arrow
778 points to Cid clusters. Time scale is h:mm:ss and the scale bar is 5 µm.

779

780 **Video 6: Wild type neuroblast exposed to Colcemid; related to Fig. S2G**

781 Wild type control (unfused) neuroblast exposed to the microtubule depolymerizing drug Colcemid,
782 expressing the membrane marker mCherry::CAAX (white), the microtubule binding protein
783 Cherry::Jupiter (white) and Cid::EGFP (Cyan). The yellow arrow points to the apical centrosome,
784 the blue arrow to Cid clusters. Time scale is h:mm:ss and the scale bar is 1 µm.

785

786 **Video 7: Cnb RNAi expressing neuroblast; related to Fig. S2I**

787 Cnb RNAi expressing (unfused) neuroblast, co-expressing the microtubule binding protein
788 Cherry::Jupiter (white) and Cid::EGFP (Cyan). The orange and blue arrow points to the apical and
789 basal centrosome, respectively. The green arrow highlights Cid clusters. Time scale is h:mm:ss and
790 the scale bar is 1 µm.

791

792 **Video 8: wild type hybrid cell; related to Fig. S3A**

793 Wild type hybrid cells expressing the microtubule binding protein Cherry::Jupiter (white) and
794 Cid::EGFP (white in single channel; Cyan in merge). The blue and orange arrow highlights
795 endogenous and ectopic Cid clusters, respectively. Time scale is h:mm:ss and the scale bar is 1 µm.

796

797

798

Video 9: Cnb RNAi expressing hybrid cell; related to Fig. S3D

Cnb RNAi expressing hybrid cell, expressing the microtubule binding protein Cherry::Jupiter (white) and Cid::EGFP (white in single channel; Cyan in merge). The blue and orange arrow highlights endogenous and ectopic Cid clusters, respectively. The yellow arrow indicates mixing of endogenous and ectopic Cid clusters. Time scale is h:mm:ss and the scale bar is 1 µm.

Video 10: wild type hybrid cell; related to Fig. 4E

Wild type hybrid cell, expressing the canonical Histone marker His2A::GFP (white). The blue and orange arrow highlights endogenous and ectopic chromosomes, respectively. The magenta arrowhead highlights the fate of missegregated chromosomes. This hybrid cell forms a heterokaryon. Time scale is h:mm:ss and the scale bar is 1 µm.